Monitoring Hydrogen Peroxide Using Electrochemically Reduced Graphene Oxide Modified Screen Printed Electrodes During Metal Assisted Chemical Etching Processes

Chun-Wen Lan (cwlan@ntu.edu.tw)
National Taiwan University https://orcid.org/0000-0003-4141-2741
Subbiramaniyan Kubendhiran
National Taiwan University
Gavin Sison
National Taiwan University
Hsiao Ping Hsu
National Taiwan University

Research Article

Keywords: Chemical etching, Reduced graphene oxide, Electrochemical reduction, Hydrogen peroxide, Copper nanoparticles.

Posted Date: March 1st, 2021

DOI: https://doi.org/10.21203/rs.3.rs-227011/v1

Abstract

The concentrations of etchant solution substituents in metal assisted chemical etching (MACE) processes control the morphology and reflectivity of subsequently etched wafers. In particular, the concentration of hydrogen peroxide (H_2O_2) plays a vital role in the MACE process. Unfortunately, the H_2O_2 concentration is not stable when prolonging the etching process at higher temperatures. As a result, the commercialization of MACE processes for the production of IP texturization has appeared industrially unattractive. Herein, we proposed an innovative method to monitor hydrogen peroxide during the MACE process with an electrochemical method. Reduced graphene oxide (RGO) prepared through an environmentally benign electrochemical method was used to modify a screen-printed electrode (SPE). Under an optimized condition, the RGO/SPE was used to test etching solutions. The MACE process was conducted and the hydrogen peroxide concentration within the etching solution was checked by the RGO/SPE. The RGO/SPE demonstrated excellent electrochemical performance and could record changes to H_2O_2 concentrations with cyclic voltammetry (CV). Interestingly, the presence of copper (Cu) in the etching solution catalyzed not only the etching process, but also the electrochemical reduction of H_2O_2. After etching, the reflectivity and structural morphology of the etched wafers were checked. The described modified electrode is disposable, and the fabrication process is rapid and inexpensive, allowing for real time application in, and control of, MACE processes.

1. Introduction

Texturization of silicon is a crucial step in solar cells fabrication processes that ultimately enhances conversion efficiencies by improving light trapping ability [1, 2]. There are currently a variety of techniques that can used for the texturization of single- and multi-crystalline silicon wafers. Anisotropic etching and isotropic etching are the two main techniques used to create upright and inverted pyramid textures on single-crystalline silicon (sc-Si) wafer surfaces [3-5]. Notably, alkaline etching techniques exhibit anisotropic behavior, and are therefore not suitable for the etching of multi- crystalline Si wafers [6]. Metal assisted chemical etching (MACE) processes have received enormous attention for its potential use in texturizing silicon wafers. So far, a variety of textures such as nanopores [7], nanowires [8], and inverted pyramid (IP) structures has been produced on the surfaces of sc-Si wafers using the MACE process [9]. Among them, the IP structure has the lowest specific surface area and has demonstrated excellent light trapping ability. As such, wafers etched in this way have low surface carrier recombination rates and produce highly efficiency solar cells [10]. In the MACE process, reaction parameters, such as reaction temperature, concentration of etchant, and reaction time, play key roles in the formation of IP textures on sc-Si surfaces [11]. Generally, copper (Cu) or silver (Ag) metal is used in the MACE process in combination with hydrofluoric acid (HF) and hydrogen peroxide (H_2O_2) [12]. However, evaporation of H_2O_2 readily occurs during the etching process, especially at high temperatures [13]. Our recent study reveals that the subsequent changes to H_2O_2 concentration incurs variations in surface morphology and reflectivity of the etched wafers [14]. Hence, it is necessary to monitor the changes in the H_2O_2 concentration of the etching solution during the throughout process in order to maintain constant concentrations.

Several analytical methods including electrochemical [15], titrimetry [16], spectrophotometry [17], chemiluminiscene [18], and fluorimetry [19] have been used for the detection of H_2O_2 [20]. Of these, the electrochemical method is relatively simple, cost-effective, rapid, and sensitive when compared to the other listed detection methods [21]. However, unmodified electrodes are unsuitable for the detection of analytes due to their high electron transfer impedance and poor catalytic activity [22]. Therefore, electrode modification with suitable electrode materials is crucial. Graphene as two-dimensional honeycomb sp^2-hybridized nano sheets with single atom thickness is a potential candidate [23, 24]. To date, graphene has been used for the fabrication of bio and electrochemical sensors due to its high electrical conductivity, specific surface area (2600 m^2/g), charge carrier mobility, flexibility, and mechanical strength; all of which are more ideal than the properties other carbon nanomaterials [25, 26]. Thus, electrochemically reduced graphene oxide (RGO) was used for the fabrication of various modified electrodes. The preparation of RGO with an electrochemical method is eco-friendly, rapid, and more conducting than chemical reduction [27]. To date, H_2O_2 detection methods have only been demonstrated only in biological based samples with no reports for the detection of H_2O_2 in a harsh environment, such as etching solution [28, 29].

In this work, the concentration changes of H_2O_2 during the MACE process were detected with an electrochemical method. Initially, the copper MACE method was conducted to produce the IP textured wafers. The morphology and reflectivity of the etched wafers were investigated. Then, the stability of spent etching solution was monitored by electrochemical detection using an RGO-modified disposable screen-printed electrode. Finally, the solution concentration difference determined by peak current response changes of the electrodes was remade with the introduction of new H_2O_2. After makeup, the etching process was conducted again using the same procedure. The morphology and reflectivity changes were recorded and compared with the results of fresh solution.

2. Experimental

2.1 Materials and methods

Graphene oxide, copper sulfate ($Cu(SO_4).5H_2O$, 99.99%), sodium phosphate mono basic (NaH_2PO_4) and sodium phosphate di basic (Na_2HPO_4) were received from Echo Chemical Co. Hydrofluoric acid (HF, 49%), hydrogen peroxide (H_2O_2, 30%), nitric acid (HNO_3, 70%) were purchased from Renew Chemical Materials Co. The supporting electrolyte, 0.05 M phosphate buffer, was prepared by dissolving Na_2HPO_4 and NaH_2PO_4 in DI water. All reagents were used without further purification. The screen printed electrodes (SPE) were purchased from Zensor R&D Co.. The surface morphologies of the etched wafers and modified electrodes were investigated using an FEI Nova nano scanning electron microscope (SEM) 230 equipped with an EDAX Apollo silicon drift detector energy dispersive X-ray spectroscopy system. A Laser Raman spectrometer (Jasco NRS-5100) was used to examine the defects and disorders of the electrode materials. The electrochemical studies were performed using a CHI1211C instrument. The CHI instruments worked based on a conventional three electrode system using SPE consist of the graphite as

a working electrode, saturated Ag/AgCl (saturated KCl) as a reference electrode, and graphite wire as a counter electrode.

2.2 Cu assisted chemical etching of sc-Si

Boron doped p-type as-cut sc-Si wafers with thickness of 165 µm, (100)-oriented surface, and resistivity 0.5- 1.5 Ω.cm, sliced into 100 mm × 50 mm sheets were used in this study. Prior to etching, the wafers were cleaned using 10% HF for 10 min to remove any native oxides. Thereafter, wafers were immersed in a 0.06M $Cu(SO_4).5H_2O$/2M HF/1M H_2O_2 etching solution in a bubbling bath environment for 7 min to produce the desired IP texturizations. After etching, the wafers were immersed in a H_2O: HNO_3 (1:1) solution under sonication for 30 min. Finally, the etched silicon wafers were thoroughly rinsed with DI water, dried, and characterized. Additional wafers were further etched in the same solution after 30 and 60 min to check the stability of the etchant.

2.3 Fabrication of RGO modified electrodes

The GO was prepared by a modified Hummer's method based on previous reports [30]. Initially, about 7 µL of the GO (0.15 mg/mL) solution was drop cast on the pre-cleaned SPEs and dried using a hot plate. Finally, the GO was reduced electrochemically in the phosphate buffer solution (pH-5) at a 50 mV/s scan rate for 5 cycles in the potential window of 0 to -1.6V. Then, the modified electrode was dried and used for the real time detection of H_2O_2 in the etching solution. Fig. 1 shows the schematic of electrode fabrication and measurement.

3. Results And Discussion

The surface morphology of the MACE processed wafers were checked by SEM with corresponding images shown in Fig. 2. The raw wafer had grooves and the saw marks on the surface before etching (Fig. 2(a)). After etching at 60 °C for 7 min in fresh etching solution, random IPs were observed on the surface (Fig. 2(b)). The surface morphology of the subsequent etched wafers in spent etching solution after 30 min and 60 min were irregular and collapsed, as shown in Figs. 2(c) and 2(d), respectively, due to the evaporation of H_2O_2. During the etching process, Cu^{2+} ions were reduced as nanoparticles (NP) by electrons donated from the silicon substrate which allowed the Cu-NPs to deposit onto the silicon wafer surface [8]. Then, the Cu-NPs enticing the Cu^{2+} ions in the etching solution led to the aggregation of Cu NPs [31]. Hence, the silicon surface was oxidized and dissolved in the etching solution upon reacting with HF.

IP structures formed on the Si wafer surface after the acidic environment reacted with the holes injected by H_2O_2 via the copper NPs into the silicon [32]. At lower concentrations of H_2O_2, the rate of hole injection and the rate of etching in silicon beneath the Cu-NPs simultaneously decreases. The reflectance spectra of the etched wafers were checked and are correspondingly shown in Fig. 3. Due to poor light trapping, the raw wafers exhibited a high reflectivity of about 32.1%. After etching, the reflectivity

decreased due to the formation of IP textures on the surface. The formation of IP structures could increase the light travelling path with a triple bounce on the adjoining (111) side walls of IP [33]. However, the reflectivity of the wafers etched after 30 and 60 min increased due to the significant changes in the adjoining facet planes of IP. This indicated that the reflectivity and morphology deteriorated when the etching was prolonged for longer periods of time.

3.1 Surface morphology and Raman spectra of the modified and unmodified electrodes

The surface morphologies of the bare, modified, and unmodified electrodes are shown in Figs. 4(a)-4(c). Flake-like structures were observed for the unmodified SPE. The observation of a crumbly thin layer on the electrode confirmed surface modification with GO. Further, wrinkles and a shrunken sheet-like structure were attributed the electrochemical reduction of the GO.

Raman spectroscopy is an important tool used to characterize carbon-based nanomaterials, such that the presence of conjugated and double carbon–carbon bonds increases Raman intensities [34, 35]. Fig. 5 depicts the Raman spectra of bare SPE, GO/SPE and RGO/SPE. The Raman spectra of the modified electrode shows two major peaks assigned for D (disorder) and G (graphitic) bands. The D band (1359 cm^{-1}) is associated with the defects and disorder of the sp^2 carbon lattice, and the G band (1587 cm^{-1}) is due to the graphitic nature and highly ordered arrangement and of sp^2 carbon [36].

As shown in Fig. 5, owing to the graphitic nature, the intensity of the G band (1587 cm^{-1}) is higher than the D band (1359 cm^{-1}). When the electrode was modified with GO, the intensity of the D band increased due to the disorder in the SP^2 carbon by the formation of oxygen functional groups. The intensity of the D band was further increased past the G band due to the formation of defects and disorders during electrochemical reduction. Moreover, the intensity ratios (I_D/I_G) of the bare SPE, GO/SPE, RGO/SPE were calculated to be about 0.26, 0.43, and 1.43, respectively. Significantly, the higher intensity ratio of RGO indicated that the reduction process changed the structure of GO by creating more structural defects [37].

3.2 Electrochemical performance of the modified and unmodified electrodes

The electrochemical performances of the electrodes were checked in a 0.05 M phosphate buffer (pH-3) solution at a scan rate of 50 mV/s. Initially, the etching solution was prepared by mixing 0.06 M $CuSO_4$, 2M HF, and 1M H_2O_2 in 200 mL of water (solution-a). Then, the prepared solution was diluted 10 times with water (solution-b). About 250 µL of the etching solution (solution-b) was scanned with final concentrations of 5 mM H_2O_2 and 300 µM $CuSO_4$. For comparison, etching solutions were prepared separately without $CuSO_4$ (solution-c) and H_2O_2 (solution-d). As shown in Fig. 6(a), the RGO/SPE showed cathodic peaks at -0.4 V (small) and -0.8 V, and an anodic peak at -0.11 V. A well-defined cathodic peak with a high peak current response at -0.8 V was attributed to the electro reduction of H_2O_2. The peaks at -0.4 V and -0.8 V were due to the redox behavior of Cu^{2+} ions in the etching solution [38]. To confirm the redox behavior of Cu^{2+} ions, the etching solutions (c and d) were checked separately. When adding solution-c without $CuSO_4$, the cathodic peak was observed at -0.69 V which corresponded to the reduction

of H_2O_2 and no redox peaks were found in the applied potential window (Fig. 6(b)). The RGO/SPE had redox peaks during the addition of solution-d without H_2O_2 (Fig. 6(c)). This result confirmed the redox behavior of Cu present in the etching solution. The electrochemical response was poor with the separate addition of 5 mM H_2O_2. However, the RGO/SPE exhibited a well-defined irreversible cathodic peak with high peak current response with the addition of 5 mM H_2O_2 with 300 µM $CuSO_4$ ((Fig. 6(d)).

Previously, Cu based nanocomposites were used as an electrode modifier for the detection of H_2O_2 due to their excellent electrocatalytic properties [39, 40]. For instance, Cheng et al. [41] reported the use of the RGO/Cu_2O composite for the electrochemical detection of H_2O_2. In such, similar redox peak patterns were observed due to the presence of Cu_2O in the composite material. Similarly, the $CuSO_4$ from within the etching solution enhanced the electrocatalytic reduction of the H_2O_2 on RGO/SPE.

The electrocatalytic properties of the modified electrodes were checked in the 0.05 M phosphate buffer at pH 3. Fig. 7(a) shows the CV response of the bare SPE, GO/SPE, and RGO/SPE for the addition of 5 mM H_2O_2 from the etching solution. The RGO/SPE displayed better electrochemical performance than the bare and GO modified electrodes. Hence, the RGO/SPE was then used for real time monitoring when investigating the stability of the etchant in the MCCE process.

Furthermore, the RGO modified electrodes were prepared by CV electrochemically using different cycles such as 5 (RGO/SPE-5) and 10 (Fig. 7(b)). In comparison, the RGO/SPE-5 showed slightly higher responses than the RGO/SPE-10 cycles. Therefore, 5 cycles were used for the electrochemical reduction of GO in the fabrication process of the modified electrode. The electrochemical behavior of the RGO/SPE towards the detection of H_2O_2 was checked using different pHs values for the electrolyte. Fig. 7(c) shows the electrochemical responses of RGO/SPE at different pH values such as 3, 5, 6 and 7 for the electro reduction of 5 mM H_2O_2. Inferior electrochemical response and higher reduction potentials were observed when using pH 6 and 7. Conversely, the RGO/SPE exhibited a higher peak current response and a lower reduction potential. In particular, a well-defined and sharp cathodic peak was obtained in pH 3 rather than pH 5. Notably, the pH of the etching solution was acidic due to the etching solution containing 2 M HF. Hence, pH-3 was used for the entirety of electrochemical experiments. In order to investigate the electrocatalytic property of the RGO/SPE, different concentrations of H_2O_2 were added from the etching solution (solution-a) in the 0.05 M phosphate buffer pH 3. As shown in Fig. 7(d), the peak current responses increased gradually for each addition of H_2O_2 from 50 to 300 mM. The results indicated that the modified electrode had desirable electrocatalytic properties and was successful in the detection of the H_2O_2 in the etching solution without dilution.

3.3 Real time monitoring of RGO/SPE for etching solution stability

The etchant for IP texturization was prepared by mixing to concentrations of 0.06 M $CuSO_4$, 2 M HF, and 1 M H_2O_2 in 2 L water. Then, the etching solution was sonicated and stirred for 5 and 10 min, respectively. About 1725 mL of etching solution was poured into a plastic container and transferred to a pre-heated

water bath at 65 °C. Before heating the etching solution, a 1 mL of sample was pipetted out to check the solution's electrochemical response of H_2O_2 by CV.

The etching solution was heated until reaching 60 °C, then pre-cleaned sc-Si wafers (100 mm x 50 mm) were etched in the bath with nitrogen bubbles for 7 min. After etching, the wafers were transferred into a sonication bath containing a cleaning solution (HNO_3: H_2O (1:1)) to remove Cu NPs. Meanwhile, about 1 mL of the spent etching solution was pipetted out to check for changes in the electrochemical response. The solution was kept in the water bath and maintained at 60 °C. After 30 and 60 min time intervals, new silicon wafers were etched and solution samples were collected after etching for electrochemical analyses. Based on the changes in the peak current responses, the evaporated amount of H_2O_2 was calculated from the recovery results and the corresponding difference was added into the etching solution. After makeup with new H_2O_2, a sample was collected for analyses and etching was conducted to compare the results with those from the fresh solution. The etched wafers were dried and checked for reflectivity and morphology. Fig. 8(a) shows the electrochemical responses of the etching solution samples collected at different time intervals. The collected etching samples were analyzed by CV without further dilution. About 50 µL of (100 mM H_2O_2) from the collected samples were added into the 0.05 M phosphate buffer pH 3. The RGO/SPE exhibited a higher peak current response at about 302 µA. After etching, the peak current response decreased to 261 µA due to the evaporation of H_2O_2. The peak current responses were decreased to 207 and 161 µA for the samples collected at 30 and 60 min time intervals. These results confirmed the evaporation of H_2O_2 during the etching process. From the peak current responses, the change in H_2O_2 was calculated to be about 0.47 M. Hence, new H_2O_2 was introduced to increase the etching solution's concentration by 0.47 M. After which, the peak current response increased to appear similar to the one from the fresh solution. The changes in the reflectivity of the etched wafers were recorded and shown in Fig. 8(b). The raw wafer showed the highest reflectivity due to poor light trapping ability. After etching, the reflectivity decreased to 5.99 % which confirming the formation of well-defined IP structures on the silicon wafers surface.

Nevertheless, the reflectivity increased to 7.30 and 8.60 % for after 30 and 60 min due to structural changes on the etched wafers. Conversely, a low reflectivity of about 5.99 % was obtained again after etching in the solution with the makeup of 0.47 M H_2O_2. The structural morphology of the etched wafers was checked by SEM where the corresponding images are shown in Figs. 9(a)-9(d). Here, IP structures were clearly observed after etching for 7 min, but became irregular and merged with each other after the 30 and 60 min time intervals. The vigorous interaction of Cu^{2+} ions with the silicon wafers surfaces at low concentrations of H_2O_2 caused low inclination angles and poor anisotropy [42]. As a result, the IP structures were not clear in the prolonged solutions. Interestingly, the IP structures became clear after makeup of the solution with H_2O_2. The etching rates of the experiment were calculated using the following formulas [43],

$$\Delta S = \frac{\Delta m}{2\rho S} \quad (1)$$

$$Vavg = \frac{\Delta S}{t} \quad (2)$$

Here, Δm is total mass loss, ΔS is thickness loss, t is time, ρ is mass density, and S is surface area of the silicon wafers, respectively. The thickness lost and etching rate calculated from Eqs. (1) and (2) are tabulated in Table-1.

Table 1 Thickness loss and etching rate obtained from Eqs. (1) and (2) for different cases.

Wafer name	Initial weight (g)	Weight after Etching (g)	Thickness loss (µm)	Etching rate (µm/s)
After etching	1.844	1.667	7.59	1.11
Etching after 30 min	1.810	1.478	14.24	1.63
Etching after 60 min	1.822	1.362	19.75	2.01
Etching after makeup with 0.47 M H_2O_2	1.840	1.710	5.59	0.8

As shown in Table-1, the etching rate increased after 30 and 60 min due to the evaporation of H_2O_2. These results indicated that H_2O_2 decreased the etching rate and increased the anisotropic etching of the MACE process. At higher Cu or lower H_2O_2 concentrations, the etching rate of the reaction increased, and a dense Cu layer formed due to the aggregation of Cu NPs on the silicon surfaces. As a result, the morphology of the etched wafers changed when heating the etching solution at longer times and at high temperatures. After makeup with H_2O_2, the reaction rate decreased because the H_2O_2 controlled the aggregation by increasing oxidization rates of the Cu NPs. Hence, more well-defined IP structures were formed on the silicon surface after makeup.

4. Conclusions

The stability of the etchant solution in the MACE process was monitored with an electrochemical sensor. This simple, cost effective, and environmentally benign electrochemical method used an RGO/SPE for real time analyses of H_2O_2 during the MACE process. The presence of Cu in the etching solution facilitated the electroreduction of H_2O_2. Owing to variations in the H_2O_2 concentration, reflectivity and morphology changes were observed when prolonging the etching experiment. The rate of the MACE process and the anisotropic etching behavior was dependent on the concentration of H_2O_2. With the

addition of fresh H_2O_2 to spent etching solution, up to 60 min post fresh etch, the desired etching rate, reflectivity, and morphology of etched wafers could be observed. The amount of H_2O_2 lost due to evaporation was calculated based on the electrochemical peak current response of the RGO/SPE. This method was relatively rapid, inexpensive, simple and reliable when compared with other detection methods. Moreover, the proposed method is suitable for monitoring the stability of the etching solution in commercial production.

Declarations

Acknowledgement

This work was sponsored by the Ministry of Science and Technology (MOST) and the United Renewal Energy Co. through the Advanced Green Energy Project.

Funding (information that explains whether and by whom the research was supported)
This work was sponsored by the Ministry of Science and Technology (MOST) and the United Renewal Energy Co. through the Advanced Green Energy Project.

Conflicts of interest/Competing interests (include appropriate disclosures)
The authors declare that they have no conflicts of interest

Availability of data and material(data transparency)
Not applicable

Code availability (software application or custom code)
Not applicable

Authors' contributions (optional: please review the submission guidelines from the journal whether statements are mandatory)
All authors contributed to the study conception and design. Material preparation, data collection and analysis were performed by Subbiramaniyan Kubendhiran, Gavin Sison and Hsiao Ping Hsu. The first draft of the manuscript was written by Chung-Wen Lan and all authors commented on previous versions of the manuscript. All authors read and approved the final manuscript.

Ethics approval(include appropriate approvals or waivers)
The manuscript should not be submitted to more than one journal for simultaneous consideration.

Consent to participate (include appropriate statements)
All authors approved the final manuscript and agreed to submit it to the journal of Silicon.

Consent for publication (include appropriate statements)
All authors approved the final manuscript and agreed to submit it to the journal of Silicon.

References

1. Baker-Finch SC, McIntosh KR (2011) Reflection of normally incident light from silicon solar cells with pyramidal texture. Prog Photovoltaics 19:406–416
2. Sun PY, Tsai PC, Liang PY, Hsu HP, Sutejo A, Yang A, Lan CW (2020) Green scalable vapor texture etching for multicrystalline silicon wafers. Prog Photovolt Res Appl. 1–8. https://doi.org/10.1002/pip.3302
3. Basher MK, Mishan R, Biswas S, Khalid Hossain M, Akand MAR, Matin MA (2019) Study and analysis the Cu nanoparticle assisted texturization forming low reflective silicon surface for solar cell application. AIP Adv 9:075118
4. Chen W, Liu Y, Yang L, Wu J, Chen Q, Zhao Y, Wang Y, Du X (2018) Difference in anisotropic etching characteristics of alkaline and copper based acid solutions for single-crystalline Si. Sci Rep 8:1–8
5. Zhang Z, Shen W, Xue J, Liu Y, Liu Y, Yan P, Liu J, Tang J (2018) Recent advances in synthetic methods and applications of silver nanostructures. Nanoscale Res Lett 13:54
6. Zhao Y, Liu Y, Chen W, Wu J, Chen Q, Tang H, Wang Y, Du X (2020) Regulation of surface texturization through copper-assisted chemical etching for silicon solar cells. Sol Energy 201:461–468
7. Cao Y, Zhou Y, Liu F, Zhou Y, Zhang Y, Liu Y, Guo Y (2015) Progress and mechanism of Cu assisted chemical etching of silicon in a low Cu^{2+} concentration region. ECS J Solid State Sci Technol 4:331–336
8. Huang ZP, Geyer N, Liu LF, Li MY, Zhong P (2010) Metal-assisted electrochemical etching of silicon. Nanotechnol 21:465301
9. Wang Y, Liu Y, Yang L, Chen W, Du X, Kuznetsov A (2017) Micro-structured inverted pyramid texturization of Si inspired by self-assembled Cu nanoparticles. Nanoscale 9:907–914
10. Yang B, Lee M (2014) Mask-free fabrication of inverted-pyramid texture on single-crystalline Si wafer. Opt Laser Technol 63:120–124
11. Wang Y, Yang L, Liu Y, Mei Z, Chen W, Li J, Liang H, Kuznetsov A, Xiaolong D (2015) Maskless inverted pyramid texturization of silicon. Sci Rep 5:10843
12. Chen W, Liu Y, Wu J, Chen Q, Zhao Y, Wang Y, Du X (2019) High-Efficient Solar Cells Textured by Cu/Ag-Cocatalyzed Chemical Etching on Diamond Wire Sawing Multicrystalline Silicon. ACS Appl Mater Interfaces 11:10052–10058
13. Yang Y, Sheng G, Li S, Yu J, Ma W, Qiu J, El Kolaly W (2020) Nano-Texturing of Silicon Wafers Via One-Step Copper-Assisted Chemical Etching. Silicon 12:231–238
14. Kubendhiran S, Sison G, Hsu HP, Lan CW (2020) Copper Assisted Inverted Pyramids Texturization of Monocrystalline Silicon in a Nitrogen Bubbling Bath for Highly Efficient Light Trapping, Silicon 1–9
15. Liu T, Guo Y, Zhang Z, Miao Z, Zhang X, Su Z (2019) Fabrication of hollow CuO/PANI hybrid nanofibers for non-enzymatic electrochemical detection of H_2O_2 and glucose. Sens Actuators B Chem 286:370–376

16. Klassen NV, Marchington D, McGowan HC (1994) H_2O_2 determination by the I_3^-method and by $KMnO_4$ titration. Anal Chem 66:2921–2925
17. Matsubara C, Kawamoto N, Takamura K (1992) Oxo [5, 10, 15, 20-tetra (4-pyridyl) porphyrinato] titanium (IV): an ultra-high sensitivity spectrophotometric reagent for hydrogen peroxide. Analyst 117:1781–1784
18. King DW, Cooper WJ, Rusak SA, Peake BM, Kiddle JJ, O'Sullivan DW, Melamed ML, Morgan CR, Theberge SM (2007) Flow injection analysis of H_2O_2 in natural waters using acridinium ester chemiluminescence: method development and optimization using a kinetic model. Anal Chem 79:4169–4176
19. Chang MC, Pralle A, Isacoff EY, Chang CJ (2004) A selective, cell-permeable optical probe for hydrogen peroxide in living cells. J Am Chem Soc 126:15392–15393
20. Zhou K, Zhu Y, Yang X, Luo J, Li C, Luan S (2010) A novel hydrogen peroxide biosensor based on Au–graphene–HRP–chitosan biocomposites. Electrochim Acta 55:3055–3060
21. Nandini S, Nalini S, Manjunatha R, Shanmugam S, Melo JS, Suresh GS (2013) Electrochemical biosensor for the selective determination of hydrogen peroxide based on the co-deposition of palladium, horseradish peroxidase on functionalized-graphene modified graphite electrode as composite. J Electroanal Chem 689:233–242
22. Jimenez-Perez R, Gonzalez-Rodriguez J, González-Sánchez MI, Gómez-Monedero B, Valero E (2019) Highly sensitive H_2O_2 sensor based on poly (azure A)-platinum nanoparticles deposited on activated screen printed carbon electrodes. Sens Actuators B Chem 298:126878
23. Zhu L, Guo X, Liu Y, Chen Z, Zhang W, Yin K, Li L, Zhang Y, Wang Z, Sun L, Zhao Y (2018) High-performance Cu nanoparticles/three-dimensional graphene/Ni foam hybrid for catalytic and sensing applications. Nanotechnol 29:145703
24. Rao CNR, Sood AK, Voggu R, Subrahmanyam KS (2010) Some novel attributes of graphene. J Phys Chem Lett 1:572–580
25. Hang T, Xiao S, Yang C, Li X, Guo C, He G, Li B, Yang C, Chen HJ, Liu F, Deng S (2019) Hierarchical graphene/nanorods-based H_2O_2 electrochemical sensor with self-cleaning and anti-biofouling properties. Sens Actuators B Chem 289:15–23
26. Bolotin KI, Sikes KJ, Jiang Z, Klima M, Fudenberg G, Hone J, Kim P, Stormer HL (2008) Ultrahigh electron mobility in suspended graphene. Solid State Commun 146:351–355
27. Raj MA, John SA (2013) Fabrication of electrochemically reduced graphene oxide films on glassy carbon electrode by self-assembly method and their electrocatalytic application. Phys Chem C 117:4326–4335
28. Kubendhiran S, Thirumalraj B, Chen SM, Karuppiah C (2018) Electrochemical co-preparation of cobalt sulfide/reduced graphene oxide composite for electrocatalytic activity and determination of H_2O_2 in biological samples. J Colloid Interface Sci 509:153–162

29. Thirumalraj B, Sakthivel R, Chen SM, Rajkumar C, Yu LK, Kubendhiran S (2019) A reliable electrochemical sensor for determination of H_2O_2 in biological samples using platinum nanoparticles supported graphite/gelatin hydrogel. Microchem J 146:673–678
30. Sakthinathan S, Kubendhiran S, Chen SM, Karuppiah C, Chiu TW (2017) Novel bifunctional electrocatalyst for ORR activity and methyl parathion detection based on reduced graphene oxide/palladium tetraphenylporphyrin nanocomposite. J Phys Chem C 121:14096–14107
31. Liu Y, Lai T, Li H, Wang Y, Mei Z, Liang H, Li Z, Zhang F, Wang W, Kuznetsov AY, Du X (2012) Nanostructure formation and passivation of large-area black silicon for solar cell applications. Small 8:1392–1397
32. Jiang B, Li M, Liang Y, Bai Y, Song D, Li Y, Luo J (2016) Etching anisotropy mechanisms lead to morphology-controlled silicon nanoporous structures by metal assisted chemical etching. Nanoscale 8:3085–3092
33. Smith AW, Rohatgi A (1993) Ray tracing analysis of the inverted pyramid texturing geometry for high efficiency silicon solar cells. Sol Energy Mater Sol 29:37–49
34. Kudin KN, Ozbas B, Schniepp HC, Prud'Homme RK, Aksay IA, Car R (2008) Raman spectra of graphite oxide and functionalized graphene sheets. Nano Lett 8:36–41
35. Ferrari AC, Meyer JC, Scardaci V, Casiraghi C, Lazzeri M, Mauri F, Piscanec S, Jiang D, Novoselov KS, Roth S, Geim AK (2006) Raman spectrum of graphene and graphene layers. Phys Rev Lett 97:187401
36. Stankovich S, Dikin DA, Piner RD, Kohlhaas KA, Kleinhammes A, Jia Y, Wu Y, Nguyen ST, Ruoff RS (2007) Synthesis of graphene-based nanosheets via chemical reduction of exfoliated graphite oxide. Carbon 45:1558–1565
37. Das AK, Srivastav M, Layek RK, Uddin ME, Jung D, Kim NH, Lee JH (2014) Iodide-mediated room temperature reduction of graphene oxide: a rapid chemical route for the synthesis of a bifunctional electrocatalyst. J Mater Chem A 2:1332–1340
38. Lu J, Zhang X, Liu N, Zhang X, Yu Z, Duan T (2016) Electrochemical detection of Cu^{2+} using graphene–SnS nanocomposite modified electrode. J Electroanal Chem 769:21–27
39. Deng SY, Zhang GY, Shan D, Liu YH, Wang K, Zhang XJ (2015) Pyrocatechol violet-assisted in situ growth of copper nanoparticles on carbon nanotubes: The synergic effect for electrochemical sensing of hydrogen peroxide. Electrochim Acta 155:78–84
40. Ensafi AA, Zandi-Atashbar N, Ghiaci M, Taghizadeh M, Rezaei B (2015) Synthesis of new copper nanoparticle-decorated anchored type ligands: applications as non-enzymatic electrochemical sensors for hydrogen peroxide. Mater Sci Eng C 47:290–297
41. Cheng C, Zhang C, Gao X, Zhuang Z, Du C, Chen W (2017) 3D network and 2D paper of reduced graphene oxide/Cu_2O composite for electrochemical sensing of hydrogen peroxide. Anal Chem 90:1983–1991

42. Yang J, Shen H, Jiang Y, Sun L (2019) Controllable fabrication and mechanism study of textured ultra-thin silicon wafers via one-step Cu-assisted chemical etching. Mater Sci Semicond Process 100:79–86
43. Zhao S, Yuan G, Wang Q, Liu W, Zhang S, Liu Z, Wang J, Li J (2019) Morphology control of c-Si via facile copper-assisted chemical etching: Managements on etch end-points. Appl Surf Sci 489:776–785

Figures

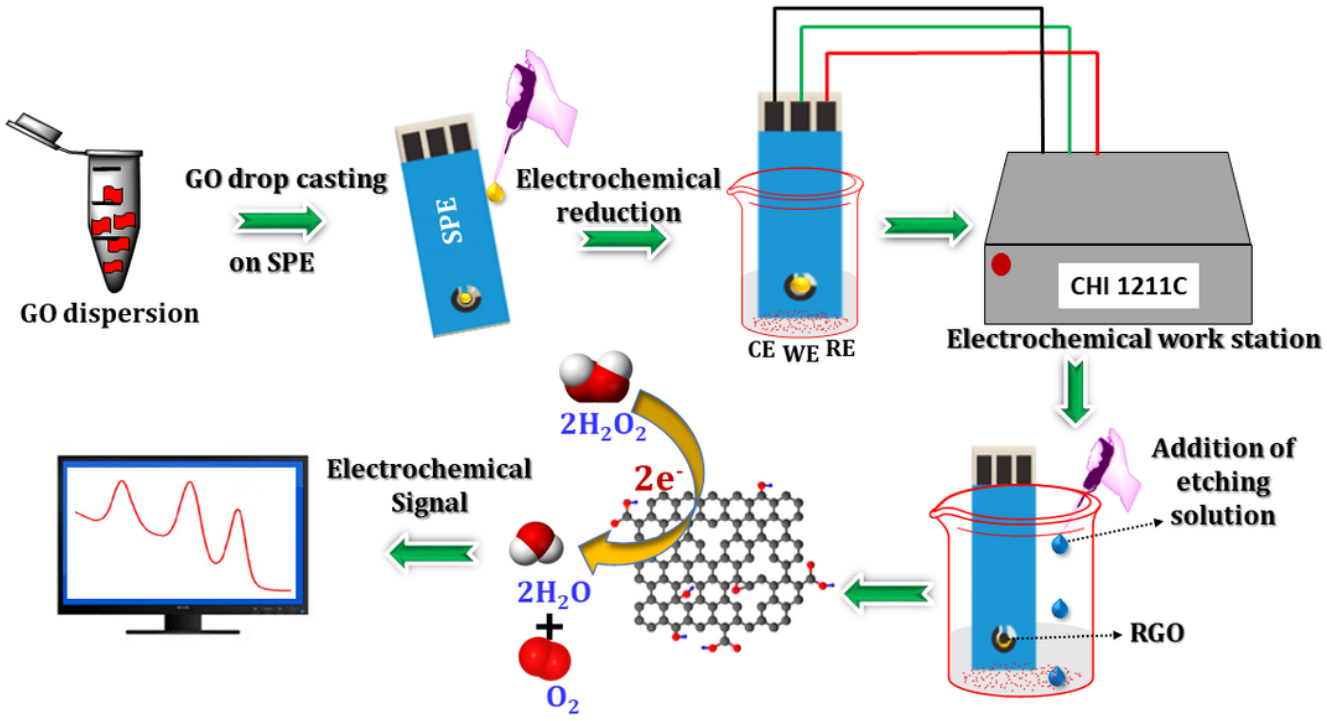

Figure 1

The schematic representation of electrode fabrication and application.

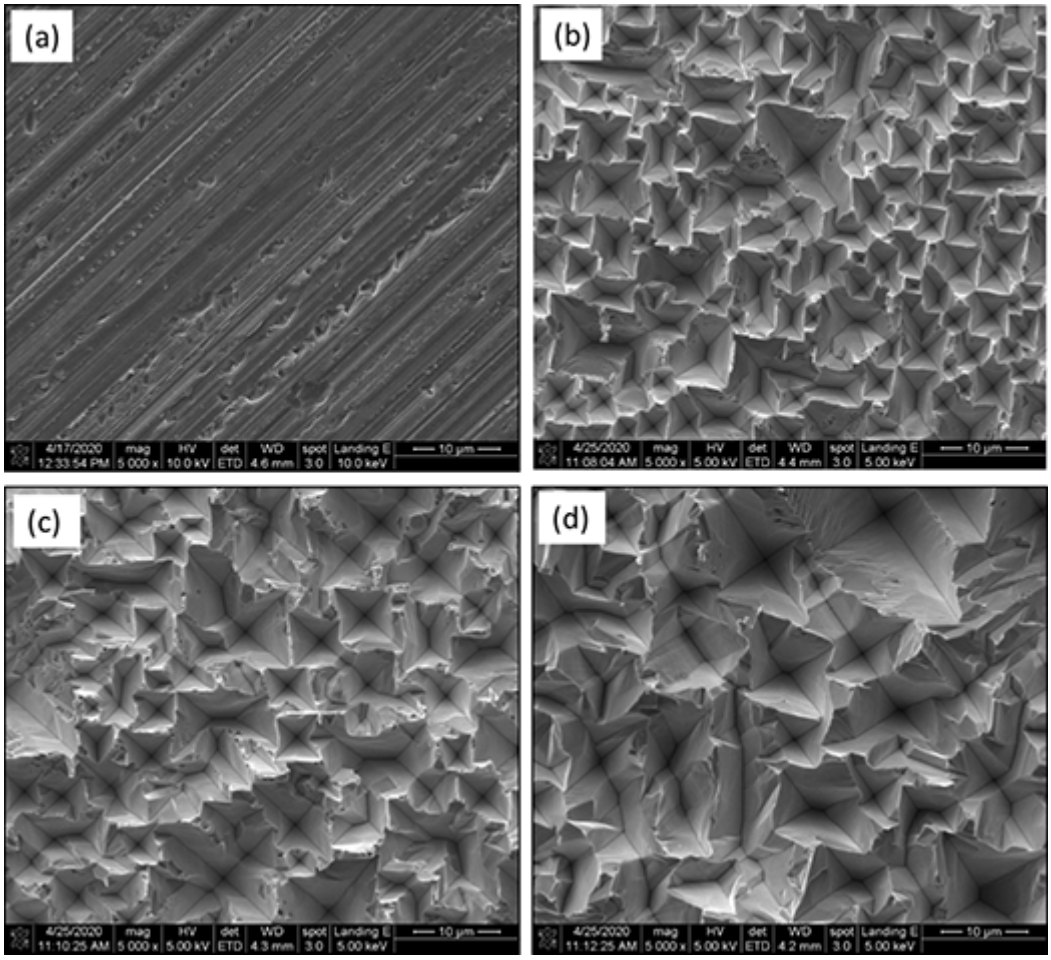

Figure 2

SEM images sc-Si wafer: (a) before etching; (b) after etching; (c) etching after 30 min; and (d) etching after 60 min in the N2 bubbling bath containing 0.06M Cu(SO4)/2M HF/1M H2O2 at 60 °C.

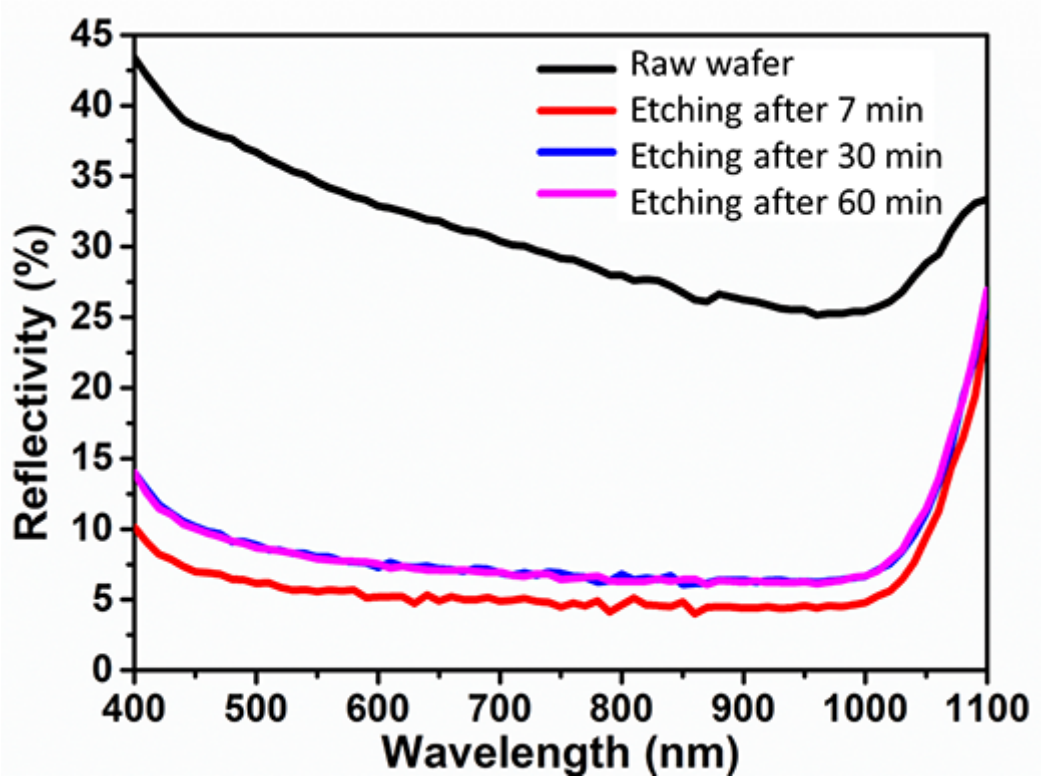

Figure 3

Reflectance spectra of IP textured wafers at different time intervals.

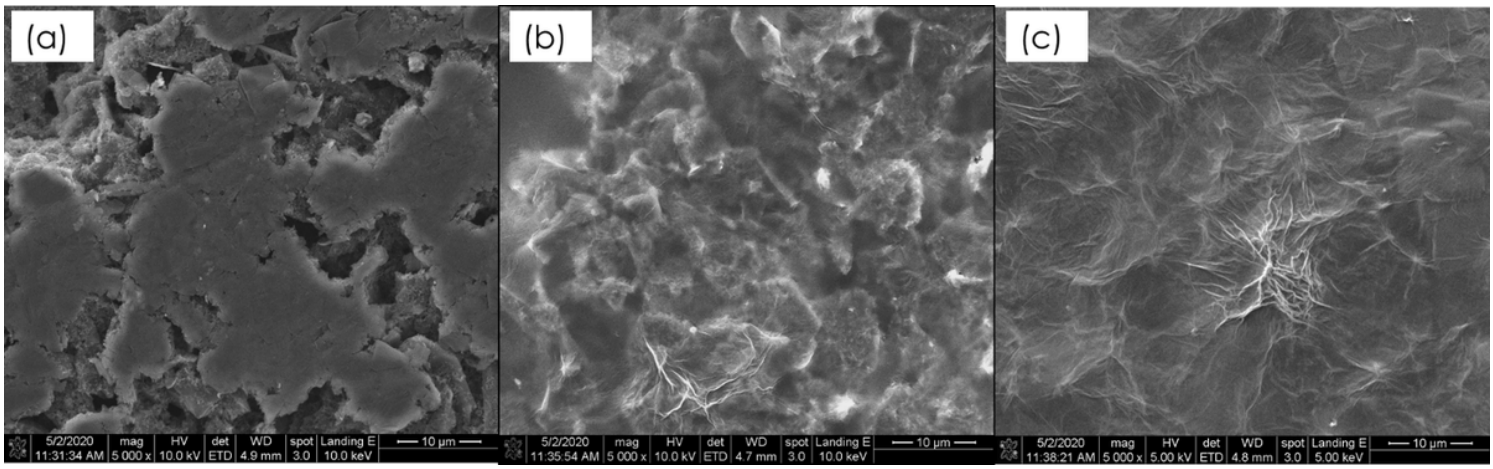

Figure 4

SEM images of (a) bare SPE, (b) GO/SPE and (c) RGO/SPE.

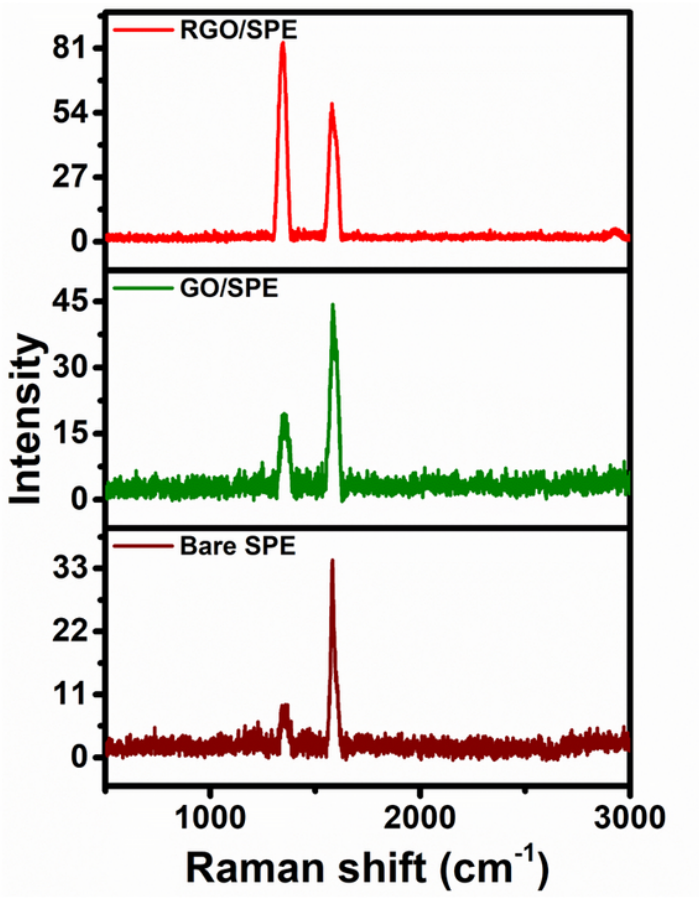

Figure 5

Raman spectra of bare SPE, GO/SPE and RGO/SPE.

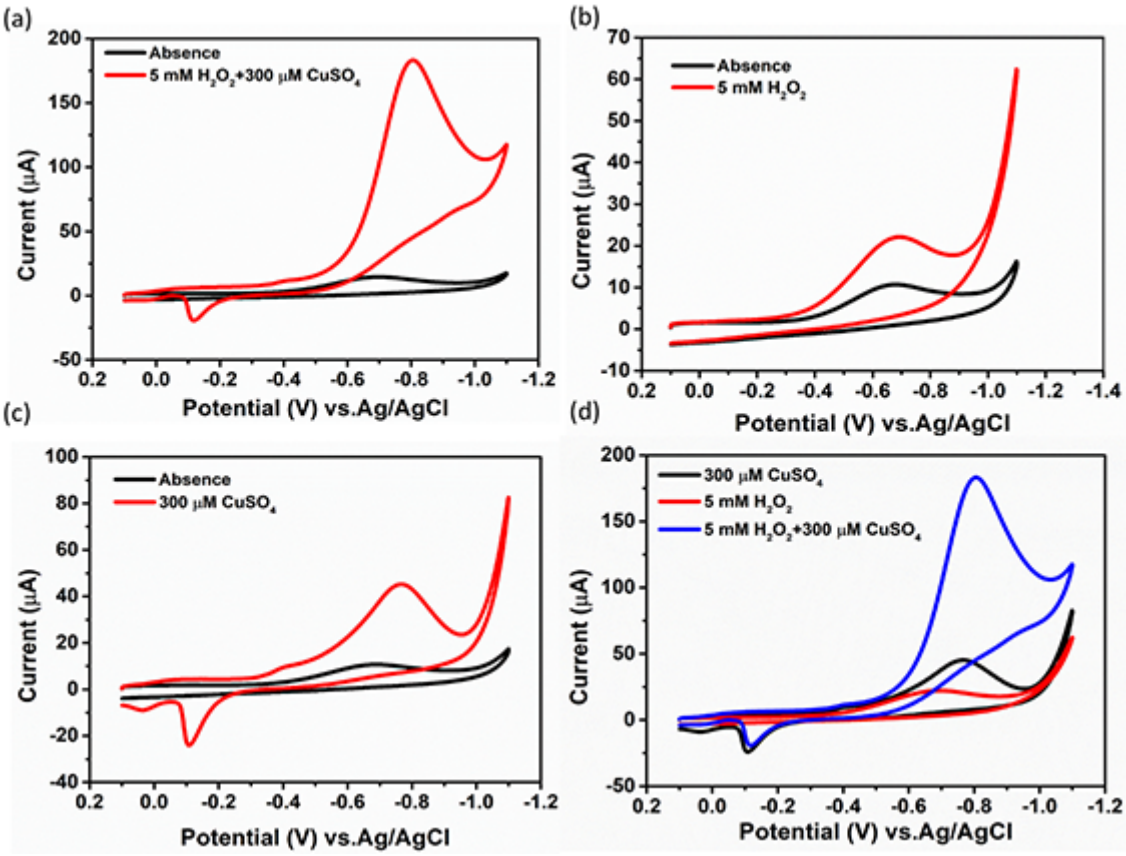

Figure 6

The CV responses of RGO/SPE for the addition 250 µL etching solution (5 mM H2O2 + 300 µM CuSO4 (a), 5 mM H2O2 from solution-c without CuSO4 (b) and 300 µM CuSO4 from solution-d without H2O2 (c) in 0.05 M phosphate buffer solution (pH 3) at a scan rate of 50 mV/S. Compassion of the electrochemical response (d).

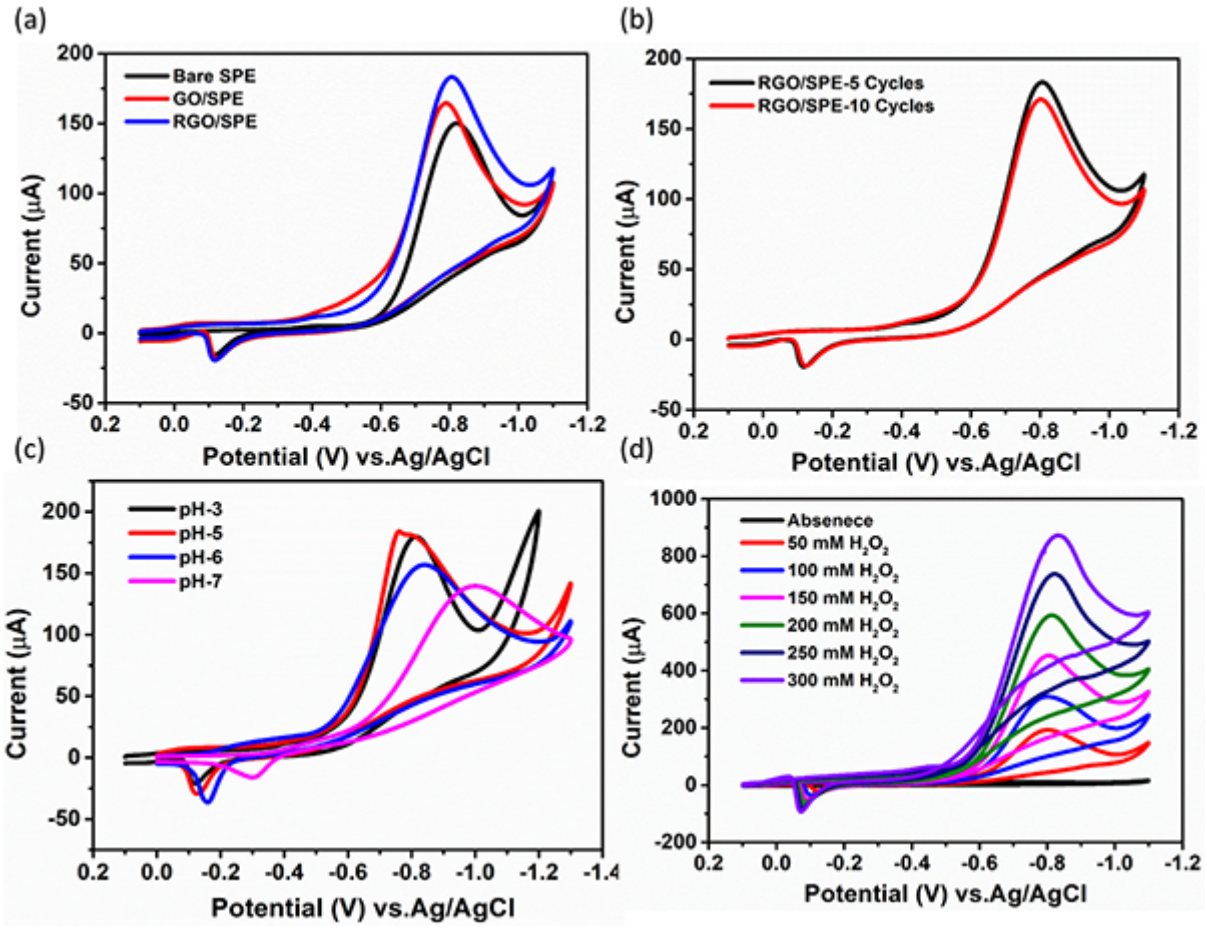

Figure 7

(a) Electrochemical responses of different films towards the detection of 5 mM H2O2 from the etching solution in 0.05 M phosphate buffer solution (pH 3) at a scan rate of 50 mV/S. (b) CV curves RGO/SPE prepared at different cycles for the detection of 5 mM H2O2 from the etching solution. (c) CV responses of RGO/SPE in phosphate buffer with different pH for the detection of 5 mM H2O2 from the etching solution. (d) CV curves obtained for the different concentration additions of H2O2 from the etching solution.

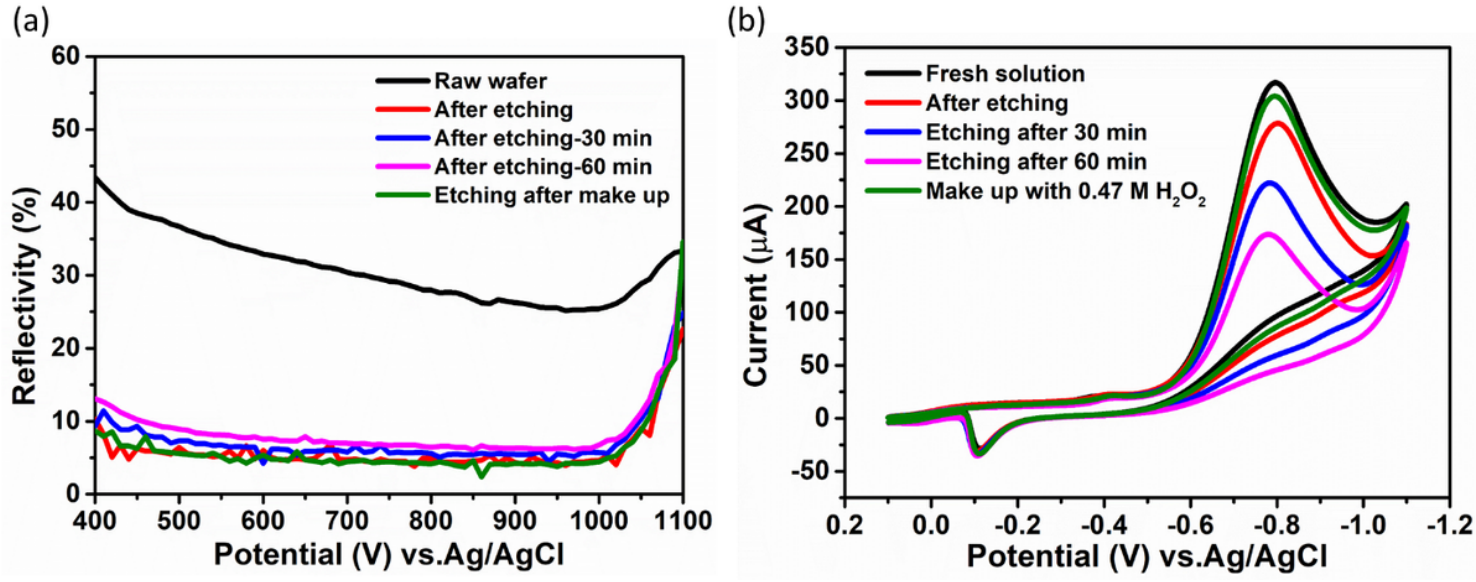

Figure 8

(a) CV responses of RGO/SPE for the addition of samples collected during the etching at different time interval in 0.05 M phosphate buffer solution (pH 3) at the scan rate of 50 mV/S. (b) Reflectance spectra of IP textured wafers at different time intervals.

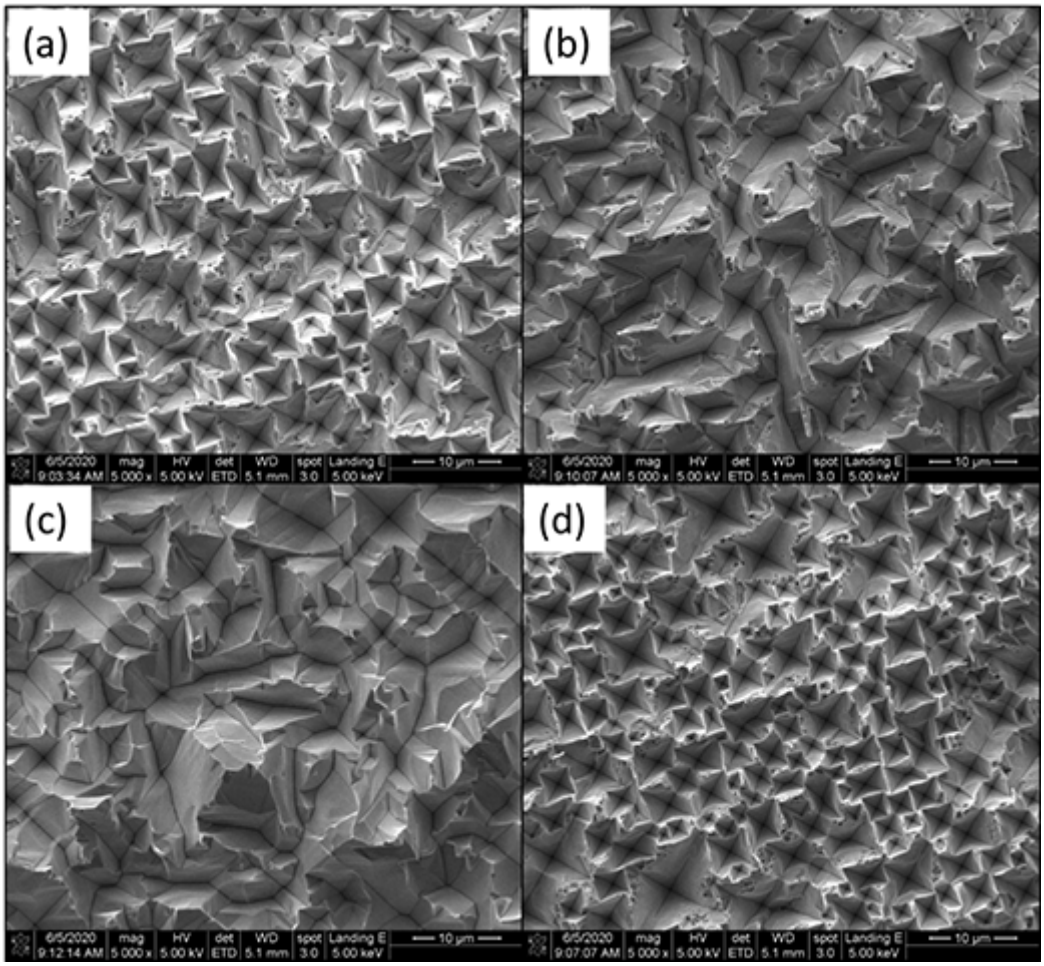

Figure 9

SEM images sc-silicon wafer (a) after initial etching, (b) etching after 30 min, (c) etching after 60 min and (d) after makeup with 0.47 M H_2O_2 in the N_2 bubbling bath containing 0.06M $Cu(SO_4)$/2M HF/1M H_2O_2 at 60 °C.